

Complete Synthetic Seismograms for High-Frequency Multimode *SH*-waves

N. FLORSCH,^{1,2} D. FÄH,^{1,3} P. SUHADOLC¹ and G. F. PANZA¹

Abstract—We present an efficient scheme to compute high-frequency seismograms (up to 10 Hz) for *SH*-waves in a horizontally stratified medium with the mode summation method. The formalism which permits the computation of eigenvalues, eigenfunctions and related integral quantities is discussed in detail. Anelasticity is included in the model by using the variational method. Phase velocity, group velocity, energy integral and attenuation spectra of a structure enable the computation of complete strong motion seismograms, which are the basic tool for the interpretation of near-source broad-band data.

Different examples computed for continental structures are discussed, where one example is the comparison between the observed transversal displacement recorded at station IVC for the November 4, Brawley 1976 earthquake and synthetic signals. In the case of a magnitude $M_L = 5.7$ earthquake in the Friuli seismic area we apply the mode summation method to infer from waveform modeling of all three components of motion of observed data some characteristics of the source.

Key words: Modal summation, broad band, Love waves, anelasticity.

1. Introduction

The mode summation method has been used (SWANGER and BOORE, 1978; PANZA, 1985; PANZA and SUHADOLC, 1987) to model the response of a flat, layered earth since Thomson and Haskell (T-H) papers appeared (THOMPSON, 1950; HASKELL, 1953). For the Rayleigh case, KNOPOFF (1964) proposed a modification of the initial T-H scheme which avoids a loss-of-precision intrinsic in the original formulation. This approach finally permitted the automatic computation of broad-band synthetic seismograms for *P-SV* waves (e.g., PANZA, 1985), which are complete in a given frequency-phase velocity window.

This paper is the expansion to *SH*-waves of the algorithm developed by PANZA (1985) and PANZA and SUHADOLC (1987) for *P-SV* waves. The loss-of-precision

¹Institute of Geodesy and Geophysics, University of Trieste, Via dell'Università 7, I-34100 Trieste, Italy.

²Currently at Laboratoire de Geophysique Applique, University of Paris 6, Paris, France.

³On leave from Institute of Geophysics, ETH, Zürich, Switzerland.

does not occur in the *SH*-wave case, while most of the other features of the *P-SV*- and *SH*-computations are practically equivalent and transposable. A first-order approximation of the anelasticity is applied including both Futterman's results based on causality analysis (FUTTERMAN, 1962) and considerations on variational methods (TAKEUCHI and SAITO, 1972; SCHWAB and KNOPOFF, 1972). This approach allows consideration of anelastic media characterized by Q as low as about 20. The attenuation effects obtained with this technique may be in error of about 0–20 percent in comparison with the exact method (SCHWAB, 1988; SCHWAB and KNOPOFF, 1971, 1972, 1973).

The "mode-follower" procedure and structure minimization as described by PANZA and SUHADOLC (1987) can be used in the *SH*-case. This approach permits the calculation of "complete" synthetic seismograms with at least three significant figures, as long as the distance to the source is greater than the wavelength (PANZA *et al.*, 1973). The seismograms computed in this way contain all the phases whose phase velocities are smaller than the *S*-wave velocity of the halfspace terminating the structural model.

The seismic source is introduced using BEN-MENACHEM and HARKRIDER'S formalism (1964) while time duration is available through a convolutive model (BEN-MENACHEM, 1961).

2. Computation of Eigenvalues

For the multimode surface-wave eigenvalue computations we make use of SCHWAB and KNOPOFF'S (1972) notation. The density-depth and velocity-depth distributions in the earth are approximated with a structure composed of a series of flat homogeneous layers. Then the dispersion function can be written as the modified product for layer-matrices (SCHWAB and KNOPOFF, 1972):

$$F_L(\omega, c) = b_n \cdot b_{n-1} \cdot b_{n-2} \cdot \dots \cdot b_1 \quad (1)$$

where n is the number of layers, including the lower halfspace. In equation (1) b_n is given by:

$$\begin{aligned} b_n &= (s, -1) && \text{if the halfspace is solid} \\ b_n &= (0, -1) && \text{if the halfspace is liquid} \\ b_n &= (1, 0) && \text{if the halfspace is rigid} \end{aligned} \quad (2)$$

For the definition of the quantity s , see Eqs. (4).

The mathematical solution of the surface wave propagation allows two types of waves in the solid halfspace, exponentially increasing and decreasing with depth. To avoid infinite values of the solution, the coefficient of the exponentially increasing wave in the halfspace must vanish.

If the halfspace is thought to be liquid, the deepest interface is at the analogy of the mantle-core boundary. Introduction of a rigid lower halfspace results in the locked mode approach (HARVEY, 1981). Then the halfspace becomes a perfect reflector and eigenvalues of the normal modes change by varying the depth of the halfspace.

b_m ($0 < m < n$) is given by:

$$\begin{aligned}
 b_m &= \left[\begin{array}{cc} \cos Q_m & \frac{\sin Q_m}{\mu_m \cdot r_{\beta_m}} \\ \mu_m \cdot r_{\beta_m} \cdot \sin Q_m & \cos Q_m \end{array} \right] & \text{if } c > \beta_m \\
 b_m &= \left[\begin{array}{cc} \cosh Q_m^* & \frac{\sinh Q_m^*}{\mu_m \cdot r_{\beta_m}^*} \\ -\mu_m \cdot r_{\beta_m}^* \cdot \sinh Q_m^* & \cosh Q_m^* \end{array} \right] & \text{if } c < \beta_m \\
 b_m &= \left[\begin{array}{cc} 1 & \frac{\omega \cdot d_m}{\mu_m \cdot c} \\ 0 & 1 \end{array} \right] & \text{if } c = \beta_m.
 \end{aligned} \tag{3}$$

In the expression (3)

- $\mu_m = \rho_m \beta_m^2$ is the rigidity of the m -th layer,
- β_m is the S -wave velocity of the m -th layer,
- ρ_m is the density of the m -th layer,
- d_m is the thickness of the m -th layer,
- ω is the angular frequency,
- c is the phase velocity.

Moreover,

$$\left. \begin{aligned}
 r_{\beta_m} &= \left(\left(\frac{c}{\beta_m} \right)^2 - 1 \right)^{1/2} \\
 Q_m &= \frac{\omega \cdot r_{\beta_m} \cdot d_m}{c} = k \cdot r_{\beta_m} \cdot d_m
 \end{aligned} \right\} \text{if } c > \beta_m$$

$$\left. \begin{aligned}
 r_{\beta_m}^* &= - \left(1 - \left(\frac{c}{\beta_m} \right)^2 \right)^{1/2} \\
 Q_m^* &= \frac{\omega \cdot r_{\beta_m}^* \cdot d_m}{c} = k \cdot r_{\beta_m}^* \cdot d_m
 \end{aligned} \right\} \text{if } c < \beta_m \tag{4}$$

$$s = -\mu_n \cdot \left(1 - \left(\frac{c}{\beta_n} \right)^2 \right)^{1/2}$$

where k is the wavenumber.

The modified matrix product of b_m and b_{m-1} in equation (1) is defined as follows:

$$[b_m \cdot b_{m-1}]_{jp} = \begin{cases} (b_m)_{jl} \cdot (b_{m-1})_{lp} & \text{if } (j+p) \text{ is even} \\ (-1)^{j+1} \cdot (b_m)_{jl} \cdot (b_{m-1})_{lp} & \text{if } (j+p) \text{ is odd.} \end{cases}$$

Seeking eigenvalues (i.e., for a given phase velocity seeking the pulsation ω) requires the determination of the roots of the dispersion function. It can be done by root-bracketing and root-refining, according to a procedure described by SCHWAB and KNOPOFF (1972). This procedure is only necessary at the beginning of each mode. For all other points, the phase velocity can be estimated by cubic extrapolation and a root-refining procedure in the F - c plane (PANZA, 1985; PANZA and SUHADOLC, 1987).

Two kinds of overflow problems can occur. The first kind of overflow can appear when Q_m^* has a large absolute value. Then the calculation of $\cosh(Q_m^*)$ and $\sinh(Q_m^*)$ is prevented. In these cases, Q_m^* has always negative values and we can assume that the following approximations hold:

$$\begin{aligned} \cosh(Q_m^*) &= \exp(-Q_m^*) \\ \sinh(Q_m^*) &= -\exp(-Q_m^*). \end{aligned}$$

In the matrix product (1) $\exp(-Q_m^*)$ can be factorized and finally set equal to one, since only the roots of the dispersion function are of interest. This operation also saves computation time. In analogy with the P - SV case (SCHWAB *et al.*, 1984), we call it the "single-layer" overflow control.

The second kind of overflow can appear when the whole matrix product (1) is computed with a phase velocity distant from the root. In this case a normalization procedure is used to prevent overflow: for each product the resulting 1×2 matrix is divided by the greatest absolute value of the matrix itself (SCHWAB and KNOPOFF, 1972). In analogy with the P - SV case (SCHWAB *et al.*, 1984), this is called the "multilayer" overflow control.

To handle realistic earth structural models, the computation scheme must allow for numerous layers in order to model possible gradients in the physical properties. Such gradients can be approximated by a sequence of thin layers. An optimized efficiency in the computations for such structures requires a mode follower and a structure minimization procedure, as described by PANZA and SUHADOLC (1987).

The structure minimization procedure is relevant to avoid computations in that part of the structure where the eigenfunction vanishes. It consists of an algorithm that keeps only the upper part of the structure for the computation, where the eigenfunction is not vanishing. This prevents a possible overflow in the calculation of eigenfunctions and saves computer time. Overflow can occur because the root is never exact and a residue remains in the exponentially increasing part of the downgoing wave.

To find the minimum of the eigenfunction above the part of the structure where overflow problems may occur, the function E_m is used. This quantity is defined as follows:

$$E_m = \rho_m \cdot \left(\frac{v_m}{v_0}\right)^2 \tag{5}$$

where v_m is the displacement at the m -th interface, ρ_m is the density of the m -th layer and v_0 is the displacement at the surface.

The maximum depth of penetration of the considered mode corresponds to the deepest minimum of E_m . The layers below the minimum can be discarded, whereas the uppermost of them define the terminating halfspace.

Generally modes are very close to each other. This creates problems in following an individual mode in the phase velocity—frequency space and in distinguishing it from the neighbouring modes. The mode follower provides an efficient way to distinguish individual modes. It is based on the fact that for a given mode, the sign of $\partial F/\partial c$ is constant, whereas in going from a mode to the next sign changes. This condition, combined with possible values of the phase velocity at a given frequency, recognizes an eventual jump to a neighbouring mode.

3. Computation of Eigenfunctions

With the geometry shown in Figure 1, the computation of the eigenfunctions at the layer interfaces can be performed as follows (see e.g., SCHWAB, 1970):

$$\begin{aligned} \begin{bmatrix} v_m \\ (\sigma_z)_m \end{bmatrix} &= \begin{bmatrix} \cos Q_m & \frac{\sin Q_m}{k \cdot \mu_m \cdot r_{\beta_m}} \\ -k \cdot \mu_m \cdot r_{\beta_m} \cdot \sin Q_m & \cos Q_m \end{bmatrix} \cdot \begin{bmatrix} v_{m-1} \\ (\sigma_z)_{m-1} \end{bmatrix} \quad \text{if } c > \beta_m \\ \begin{bmatrix} v_m \\ (\sigma_z)_m \end{bmatrix} &= \begin{bmatrix} \cosh Q_m^* & \frac{\sinh Q_m^*}{k \cdot \mu_m \cdot r_{\beta_m}^*} \\ k \cdot \mu_m \cdot r_{\beta_m}^* \cdot \sinh Q_m^* & \cosh Q_m^* \end{bmatrix} \cdot \begin{bmatrix} v_{m-1} \\ (\sigma_z)_{m-1} \end{bmatrix} \quad \text{if } c < \beta_m \tag{6} \\ \begin{bmatrix} v_m \\ (\sigma_z)_m \end{bmatrix} &= \begin{bmatrix} 1 & d_m \\ 0 & \mu_m \end{bmatrix} \cdot \begin{bmatrix} v_{m-1} \\ (\sigma_z)_{m-1} \end{bmatrix} \quad \text{if } c = \beta_m \end{aligned}$$

where v_m is the displacement and $(\sigma_z)_m$ the stress at the interface m . Notice that:

$$\dot{v} = i\omega v.$$

These computations are performed using the initial values $(v_0, (\sigma_z)_0) = (1, 0)$ at the free surface.

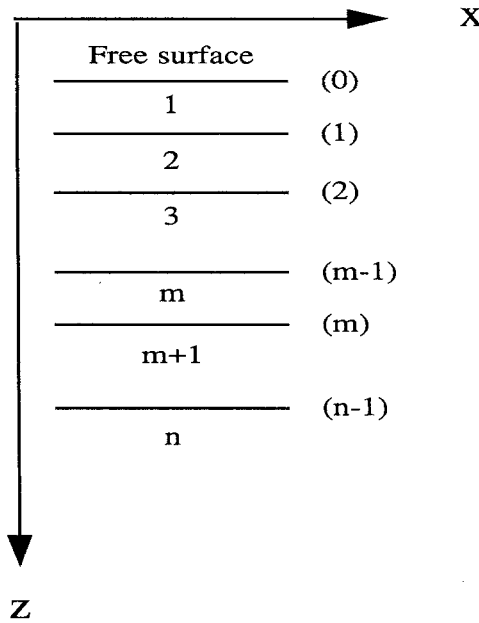


Figure 1

Coordinate system and geometry for the Love wave problem. The numbers denote layers, while the numbers in brackets denote interfaces.

As far as the phase velocity has been computed with high accuracy, the problem with “multilayer” overflow should not occur. However, “single-layer” overflow has to be expected because it depends on the thickness of the layer. By splitting each of the thickest layers in a series of equally thin layers this problem can be avoided.

4. Group Velocities

For a general background on the subject we refer to SCHWAB and KNOPOFF (1972). The group velocities are computed using the formula:

$$u = \frac{c}{1 - \frac{dc}{d\omega} \cdot \frac{\omega}{c}} \tag{7}$$

The ratio $dc/d\omega$ is calculated according to the implicit function theory:

$$\frac{dc}{d\omega} = - \frac{\left[\frac{\partial F}{\partial \omega} \right]_c}{\left[\frac{\partial F}{\partial c} \right]_\omega} \tag{8}$$

Since the *S*-wave velocities are frequency-dependent, all derivatives imply partial derivatives with respect to frequency. All required quantities are given in Appendix A.

Even if the dispersion function has been normalized to prevent “multilayer” overflow, it is not necessary to introduce the derivatives of the normalization coefficients to compute the group velocities. In fact the dispersion function without normalization is given by:

$$F_L(\omega, c) = \prod_{i=1}^n b_i(\omega, c)$$

where b_i is the matrix defined by (1), (2) and (3). This equation can be written in a recursive form (decreasing):

$$\begin{aligned} F_j &= F_{j+1} \cdot b_j \\ F_n &= b_n. \end{aligned} \tag{9}$$

Normalization leads to the division of each b_i by a coefficient g_i , which is the greatest absolute value of the elements of the resulting 1×2 matrix F_i . Therefore the normalized dispersion function is written:

$$\hat{F}_L(\omega, c) = \prod_{i=1}^n \frac{b_i(\omega, c)}{g_i(\omega, c)}. \tag{10}$$

Hence:

$$\frac{\partial \hat{F}_L}{\partial c} = \frac{\partial F_L}{\partial c} \cdot \prod_{i=1}^n \frac{1}{g_i} + F_L \cdot \frac{\partial}{\partial c} \left(\prod_{i=1}^n \frac{1}{g_i} \right).$$

A similar relation holds for $\partial \hat{F}_L / \partial \omega$. Therefore, we obtain:

$$\frac{dc}{d\omega} = - \frac{\left[\frac{\partial \hat{F}_L}{\partial \omega} \right]_c}{\left[\frac{\partial \hat{F}_L}{\partial c} \right]_\omega} = - \frac{\left[\frac{\partial F_L}{\partial \omega} \right]_c \cdot \prod_{i=1}^n \frac{1}{g_i} + F_L \cdot \frac{\partial}{\partial \omega} \left[\prod_{i=1}^n \frac{1}{g_i} \right]}{\left[\frac{\partial F_L}{\partial c} \right]_\omega \cdot \prod_{i=1}^n \frac{1}{g_i} + F_L \cdot \frac{\partial}{\partial c} \left[\prod_{i=1}^n \frac{1}{g_i} \right]}. \tag{11}$$

If the phase velocity has been computed with high accuracy, then F_L is very close to zero and (11) reduces to:

$$\frac{dc}{d\omega} = - \frac{\left[\frac{\partial \hat{F}_L}{\partial \omega} \right]_c}{\left[\frac{\partial \hat{F}_L}{\partial c} \right]_\omega} = - \frac{\left[\frac{\partial F_L}{\partial \omega} \right]_c \cdot \prod_{i=1}^n \frac{1}{g_i}}{\left[\frac{\partial F_L}{\partial c} \right]_\omega \cdot \prod_{i=1}^n \frac{1}{g_i}} = - \frac{\left[\frac{\partial F_L}{\partial \omega} \right]_c}{\left[\frac{\partial F_L}{\partial c} \right]_\omega}. \tag{12}$$

This equation does not hold if the derivative $\partial F / \partial c$ is computed away to the root of F , as in the case, where $\partial F / \partial c$ is used in the root-refining procedure of the dispersion function. In this situation a recursive approach has been chosen.

Equation (10) can be written in a recursive form as equation (9):

$$\hat{F}_j = \frac{\hat{F}_{j+1} \cdot b_j}{g_j}$$

$$\hat{F}_n = b_n$$

where b_n and \hat{F}_j are 1×2 matrices, b_j is a 2×2 matrix and g_j is a scalar value. The normalization has not been performed for the halfspace ($j = n$). The derivative of the normalized dispersion-function can now be determined with the same recursive scheme:

$$\begin{aligned} \frac{\partial \hat{F}_j}{\partial c} &= \frac{\partial \hat{F}_{j+1}}{\partial c} \cdot \frac{b_j}{g_j} + \hat{F}_{j+1} \cdot \frac{\partial}{\partial c} \left(\frac{b_j}{g_j} \right) \\ &= \frac{\partial \hat{F}_{j+1}}{\partial c} \cdot \frac{b_j}{g_j} + \hat{F}_{j+1} \cdot \frac{\frac{\partial b_j}{\partial c} \cdot g_j - b_j \cdot \frac{\partial g_j}{\partial c}}{g_j^2} \\ \frac{\partial \hat{F}_n}{\partial c} &= \frac{\partial b_n}{\partial c} \end{aligned}$$

5. Energy Integral

This additional quantity is necessary for the computation of seismograms (PANZA and SUHADOLC, 1987). The energy integral is defined as:

$$I_1 = \int_0^\infty \rho \cdot \left(\frac{\dot{v}(z)}{\dot{v}_0} \right)^2 dz. \quad (13)$$

The energy integral can be calculated analytically, since simple analytic expressions are known for the eigenfunction $v(z)$. The details of these calculations are given in Appendix B.

6. Attenuation Due to Anelasticity

The treatment of anelasticity requires, for causality reasons, the introduction of body wave dispersion (FUTTERMAN, 1962). In a medium with constant Q , the SH phase velocity can be expressed as:

$$B_1(\omega) = \frac{B_1(\omega_0)}{1 + \frac{2}{\pi} \cdot B_1(\omega_0) \cdot B_2(\omega_0) \cdot \ln\left(\frac{\omega_0}{\omega}\right)}. \quad (14)$$

The layer index m is omitted. $B_1(\omega_0)$ and $\beta_2(\omega_0)$ are the S -wave velocity and the S -wave phase attenuation at the reference angular frequency ω_0 . The quantities B_1 and B_2 are related to the complex body-wave velocity β (SCHWAB and KNOPOFF, 1972):

$$\frac{1}{\beta} = \frac{1}{B_1} - i \cdot B_2.$$

In the computation we have chosen the reference angular frequency $\omega_0 = 2\pi$ radians. In anelastic media the surface wave phase velocity c must be also expressed as a complex quantity:

$$\frac{1}{c} = \frac{1}{C_1} - i \cdot C_2$$

with C_1 the attenuated phase velocity and C_2 the phase attenuation, the latter being necessary for the computation of seismograms. C_2 can be estimated by using the variational technique (TAKEUCHI and SAITO, 1972; AKI and RICHARDS, 1980). The phase attenuation C_2 is given by:

$$C_2 = \frac{\int_0^{\infty} \mu \cdot B_1 \cdot B_2 \cdot \left(\frac{\sigma_z^2}{\mu^2 \cdot k^2} + v^2 \right) dz}{c \int_0^{\infty} \mu \cdot v^2 dz}. \quad (15)$$

This integral can be calculated analytically, since simple analytic expressions are known for the eigenfunctions. The details of this computation are given in Appendix B.

The most important effect of the attenuation is the modification of the wave velocities and the decay of amplitude in the final computations of seismograms. As the variational technique is only an approximate method, the Q values can be in error by as much as 0–20 percent in comparison with the exact method. This error arises mainly from the use of the elastic and, therefore, real eigenfunctions to compute the phase attenuation.

Recently DAY *et al.* (1989) showed the limits of the variational technique in the locked mode approximation, which can be obtained by limiting the model with a rigid or liquid halfspace. They showed that an error in amplitudes up to 100 percent can occur, when dealing with low Q -values. The error increases when the Q -values undergo large variations with depth. Introducing a solid halfspace in the model and using the structure minimization procedure prevents this kind of error.

7. Source

In order to include the seismic source in the computations, the formulation due to HARKRIDER (1970) and BEN-MENAHEM and HARKRIDER (1964) is used. For

the double-couple point source, the Fourier transform of the response can be written for a given mode as:

$$U_v = |\vec{n}| \cdot |R(\omega)| \cdot e^{i\Phi_0} \cdot e^{-i3\pi/4} \cdot k^{1/2} \cdot \chi(\theta, h) \cdot A_L \cdot \frac{e^{-ikr}}{\sqrt{2\pi r}} \cdot e^{-\omega r C_2} \quad (16)$$

where $R(\omega)$ is the Fourier transform of the source time function and $\Phi_0 = \arg(R(\omega))$ is the source apparent initial phase. $|\vec{n}|$ is the absolute value of the normal vector to the plane of motion, with units of length. The factor A_L is given by:

$$A_L = \frac{1}{2 \cdot c \cdot u \cdot I_1}$$

The effect of anelasticity is expressed by the term:

$$e^{-\omega r C_2}$$

$\chi(\theta, h)$ is the azimuthal dependence given by:

$$\chi(\theta, h) = i \cdot (d_1 \sin \theta + d_2 \cos \theta) + d_3 \sin 2\theta + d_4 \cos 2\theta$$

for a double-couple source,

$$d_1 = G(h) \cdot \cos \lambda \cdot \cos \delta$$

$$d_2 = -G(h) \cdot \sin \lambda \cdot \cos 2\delta$$

$$d_3 = \frac{1}{2} \cdot V(h) \cdot \sin \lambda \cdot \sin 2\delta$$

$$d_4 = V(h) \cdot \cos \lambda \cdot \sin \delta$$

θ is the angle between the strike of the fault and the epicenter-station direction, λ is the rake angle, δ is the dip angle and h is the source depth. The source geometry

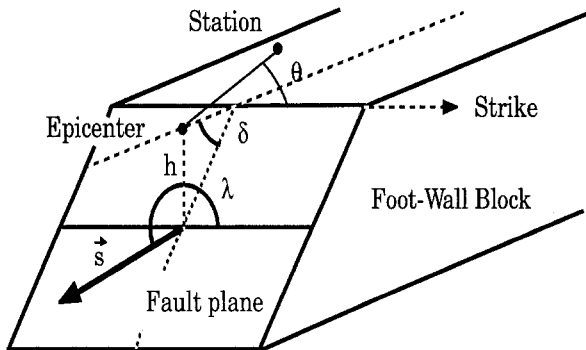


Figure 2

Source geometry and coordinate system associated with the free surface. θ is the angle between the strike of the fault and the epicenter-station direction, δ is the dip, λ is the rake and h is the source depth.

and the coordinate system associated with the free surface is given in Figure 2. $G(h)$ and $V(h)$ depend on the values of the eigenfunctions at the hypocenter:

$$G(h) = +\frac{1}{\mu_s} \cdot \left(\frac{\sigma_s^*(h)}{\dot{v}_0} \right) = \frac{1}{k \cdot \mu_s} \cdot \frac{\sigma_s(h)}{v_0}$$

$$V(h) = \frac{\dot{v}_s(h)}{\dot{v}_0} = \frac{v_s(h)}{v_0}.$$

v_0 is the value of the eigenfunction at the surface and $\sigma_s(h)$ is the stress at the depth of the source. Equation (16) is equivalent to equation (7.148) given in AKI and RICHARDS (1980). The seismogram related to a given mode is obtained by the inverse Fourier transform of (16).

8. Examples of Computation

Frequency Domain

The layered model in Table 1 represents an average structure of the Friuli seismic area in the southern pre-Alps, close to the May 6, 1976, Friuli earthquake. The same structure was used to illustrate the mode summation for Rayleigh-waves (PANZA and SUHADOLC, 1987).

Table 1
Structure FRIUL7A. Q_α is taken as $2.5Q_\beta$

Thickness [km]	Density [g/cm ³]	P-wave velocity [km/s]	S-wave velocity [km/s]	Q_β
0.04	2.00	1.50	0.60	20
0.06	2.30	3.50	1.80	30
0.20	2.40	4.50	2.50	100
0.70	2.40	5.00	2.90	200
2.00	2.60	6.00	3.30	400
3.50	2.60	6.20	3.45	400
4.50	2.60	6.00	3.35	100
10.00	2.60	5.50	3.30	50
3.50	2.60	6.00	3.50	100
2.50	2.75	6.50	3.75	400
2.50	2.80	7.00	3.85	400
7.50	2.80	6.50	3.75	100
4.00	2.85	7.00	3.85	200
3.00	3.20	7.50	4.25	400
1.50	3.40	8.00	4.50	400
9.00	3.45	8.20	4.65	400

1. Phase Velocities

The dispersion curves for the first 154 Love modes are shown in Figure 3. For S -wave velocities less than 3.35 km/s the modes are well separated. This velocity corresponds to the S -wave velocity in the upper part of the crustal low-velocity zone (LVZ). Modes situated in the part of the spectrum below this phase velocity value, sample therefore the part of the crust above the uppermost LVZ.

In the part of the spectrum with higher phase velocities the dispersion curves are packed together. An enlarged portion of this part is presented in Figure 3b. Since two LVZ are present in the structural model, areas are seen where the higher Love wave modes decompose into families of low-velocity channel waves and families of waves propagating in the upper crust. They appear in the dispersion curves as an apparent continuity of the phase velocities between adjacent modes. This mode-to-mode continuation leads to the identification of a family of waves. Each member of a wave family begins with one of the Love-wave modes and contains segments of all successive higher modes. They have almost continuous phase velocities, broken only at the points of near-oscillations. The segments of members of the family of upper-crustal waves form apparently continuous curves which sometimes seem to intersect the more horizontal trending family of the channel-wave curves. A

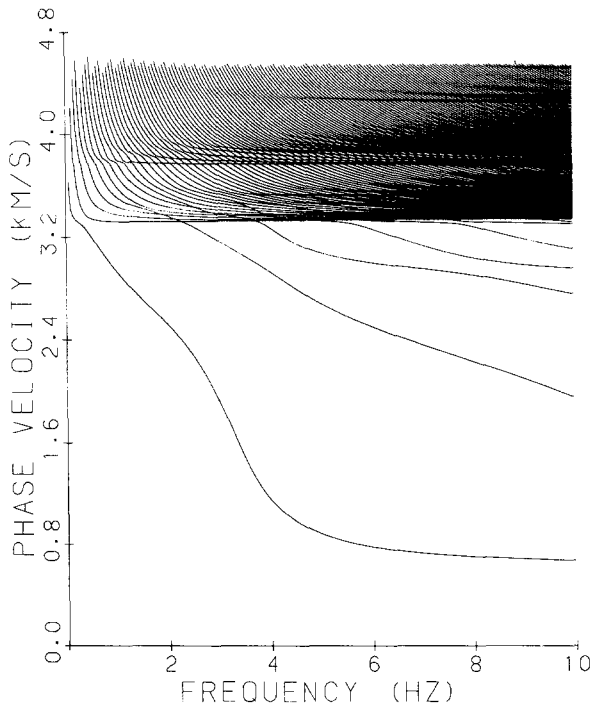


Figure 3a

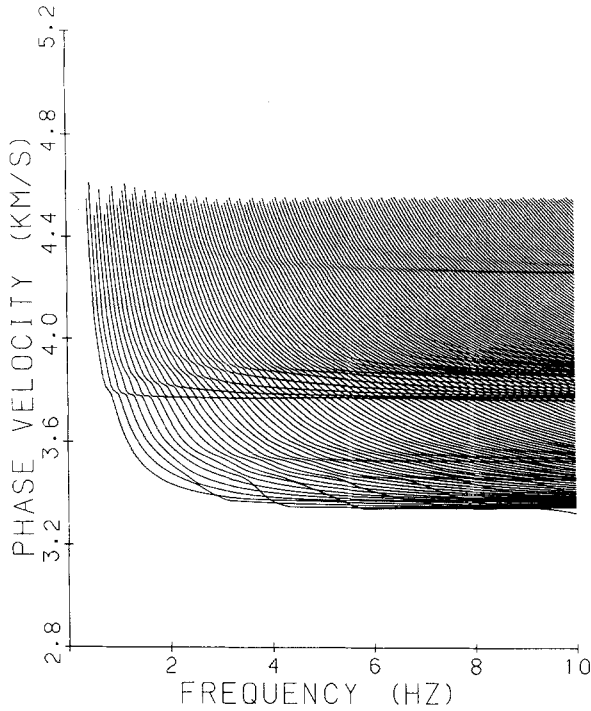


Figure 3b

Figure 3

(a) Love-wave dispersion curves for the structural model FRIUL7A. The mode numbering is the following: 0 for the fundamental mode, 1 for the first higher mode, 2 for the second higher mode, and so on up to 153. (b) Enlarged portion (modes 6–153) of part (a) showing the effect of low-velocity waveguides.

member of the family of upper-crustal waves can be identified at a frequency of about 4 Hz in the phase velocity range 3.35–3.45 km/s.

Another type of apparent continuity of the phase velocities for adjacent modes can be related to the structural layering (for example at a phase velocity of about 4.25 km/s). Such parts of the spectrum represent refracted waves at strong elastic impedance contrasts. They are characterized by phase velocities which tend to become constant with increasing frequency.

2. Group Velocities

The group velocity spectrum is presented in Figure 4. Due to the complexity of the pattern, it has been divided into two parts. Modes with group velocities less than about 2.8 km/s correspond to waves propagating in the low-velocity sediments.

In the part of the spectrum where group velocities are in the interval 2.8–3.2 km/s, several higher modes form stationary phases. They correspond to families of waves propagating in the upper crust and are characterized by the same type of mode-to-mode continuation as in the phase velocity curves. They can be interpreted as the high-frequency equivalent of *Lg* phases (SCHWAB and KNOPOFF, 1972; KNOPOFF *et al.*, 1973; PANZA and CALCAGNILE, 1975), which are propagating in the upper part of the continental crust.

The flat portions of group velocity curves formed by a large number of higher modes at about 3.35 km/s (Figure 4a) and 3.75 km/s (Figure 4b) correspond to waves propagating in the upper and lower channel.

3. Energy Integral

The energy integral can serve as an estimate of the contribution of the different modes to the surface displacement. In general, neglecting the influence of the source depth on the excitation of different modes, small values of the energy integral I_1 correspond to large surface displacements. In the whole frequency range, the fundamental mode has the lowest values of I_1 (Figure 5). For a shallow source, the fundamental mode generally dominates the surface displacement.

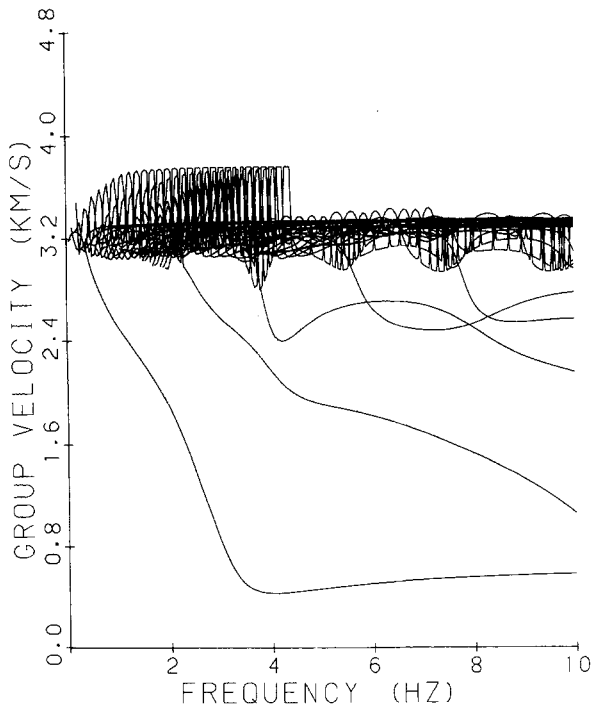


Figure 4a

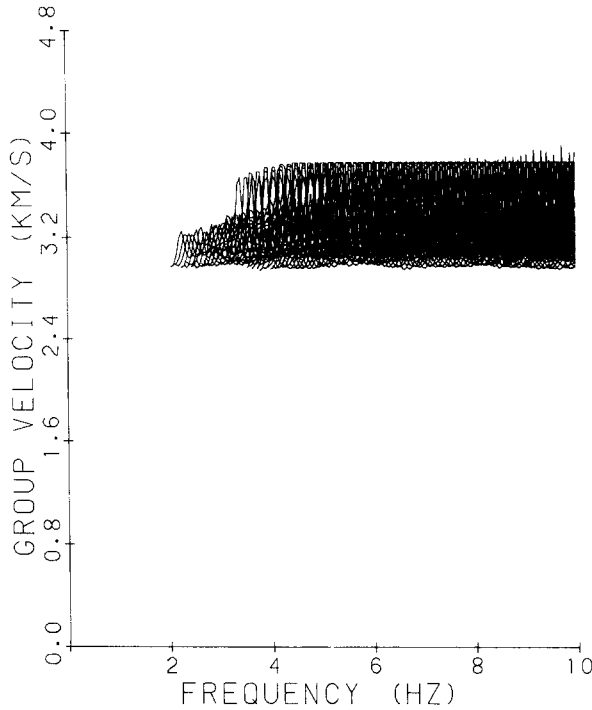


Figure 4b

Figure 4

Love-wave group velocities for the structure FRIUL7A. The spectrum is divided into two parts: a) Love modes 0–30, b) Love modes 31–153.

The mode-to-mode continuations in the lower part of the energy integral curves (Figure 5a) correspond to the high frequency equivalent of *L_g* waves. The low values of the energy integral indicate that these waves can give rise to significant amplitudes at the surface.

Most of the energy of channel waves is concentrated in the channel. Therefore, the energy integral of these families, seen in the upper part of Figure 5a, takes higher values than those for upper-crustal waves. For a given member of this family the maximum displacement in the low-velocity zone becomes larger, relative to the displacement at the free surface, with increasing frequency. Therefore, the energy integral of this member is characterized by values increasing with frequency. This can be seen in the general pattern of the upper part of Figure 5a.

4. Quality Factor Q_x

The phase attenuation C_2 of the *SH*-modes is related to the quality factor Q_x by the relation

$$1/Q_x = 2C_1 C_2$$

where C_1 is the anelastic phase velocity (SCHWAB and KNOPOFF, 1972). The quality factor is presented in Figure 6. Q_β is very low in the sedimentary layers. Modes mainly propagating in these layers are therefore characterized by low Q_x values (Figure 6a). This is the case for the first few modes, especially for the fundamental and first higher mode. The effect of layering of Q_β can be observed for several nearby modes that have almost constant Q_x , for example Q_x close to 65. The resulting Q_x values are close to the values Q_β of the structural model for those Love wave modes, whose eigenfunction mainly sample the corresponding part of the structure.

Time Domain

The first example corresponds to the November 4, 1976 Brawley, California earthquake. The structural model and source parameters have been proposed by HEATON and HELMBERGER (1978). Their structural model is given in Table 2. Since SWANGER and BOORE (1978) computed synthetic seismograms for this event with the mode-summation technique, their result, even if limited to the elastic case, provides a test for our programs. Therefore, the source parameters used to compute synthetics are the same as those given by SWANGER and BOORE.

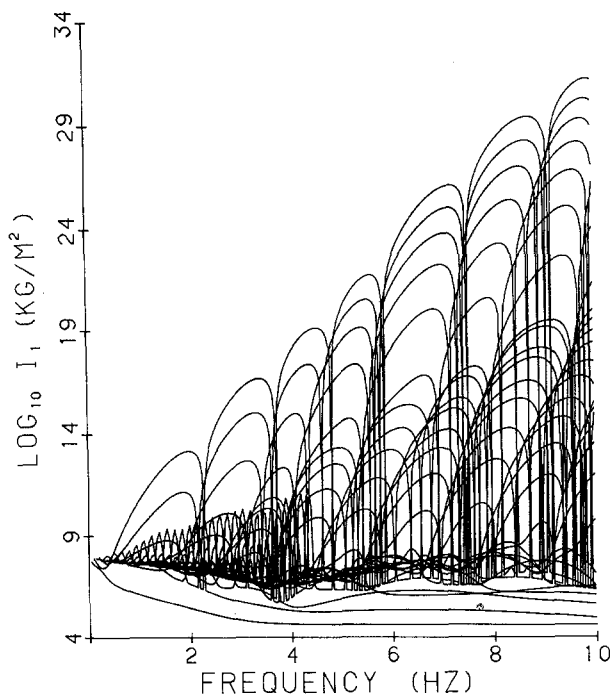


Figure 5a

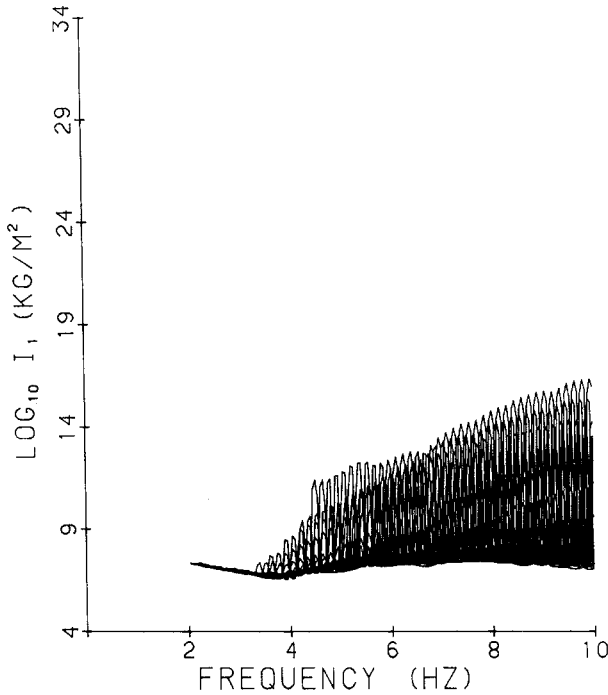


Figure 5b

Figure 5

Love-wave energy integral I_1 for the structure FRIUL7A. The spectrum is divided into two parts: a) Love modes 0–30, b) Love modes 31–153.

A strike-slip point source is placed on a vertical plane at 6.9 km depth. The rupture-velocity time-function is a symmetrical triangle with a base of 1.5 seconds. At a distance of 33 km from the source, the displacement consists almost entirely of the fundamental mode and the first higher modes (Figure 7). The recorded displacement at the station IVC, 33 km from the source, is given in the same figure. The upper frequency limit is 1 Hz. It can be seen that there is generally a very good agreement between the two synthetic signals.

Table 2

Imperial Valley Structure proposed by HEATON and HELMBERGER (1978)

Layer	Thickness [km]	Density [g cm ⁻³]	S-velocity [km s ⁻¹]
1	0.95	1.80	0.88
2	1.15	2.35	1.50
3	3.80	2.60	2.40
halfspace	∞	2.80	3.70

In the second example we present synthetic seismograms for the structural model FRIUL7A shown in Table 1. The upper frequency limit is 10 Hz. The source parameters are related to those of the Friuli, May 6, 1976 earthquake (point-source approximation with the source parameters taken from SUHADOLC *et al.*, 1988). The receivers are chosen in the direction of the dominant lobe of the radiation pattern of *SH*-waves (north-east direction, with a strike-receiver angle of 235°), resulting from the selected source parameters. Synthetic ground displacements, velocities and accelerations are presented in the lower part of Figure 8. The signals are filtered with a Gaussian filter (the first filtered frequency is at 9 Hz, with a reduction of the amplitude by factor 100 at the cutoff frequency of 10 Hz). This filter prevents ringing due to the cutoff frequency. A decomposition of the displacement into different sets of modes is presented in the upper part of the figure. It shows that the higher modes are essential in defining the shape of the waveform, especially in the body wave part of the synthetic seismograms.

In Figure 9 synthetics due to a source with finite rise time are presented. The rupture-velocity time-function is a symmetrical triangle with a base of 0.5 seconds. The signals are filtered with the already described Gaussian filter. As expected, the energy is shifted to lower frequencies, as the duration of the source is increased. The

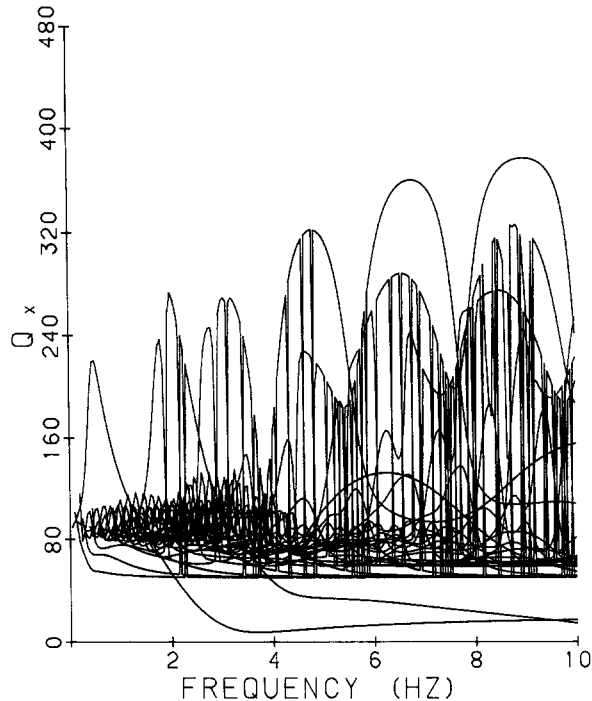


Figure 6a

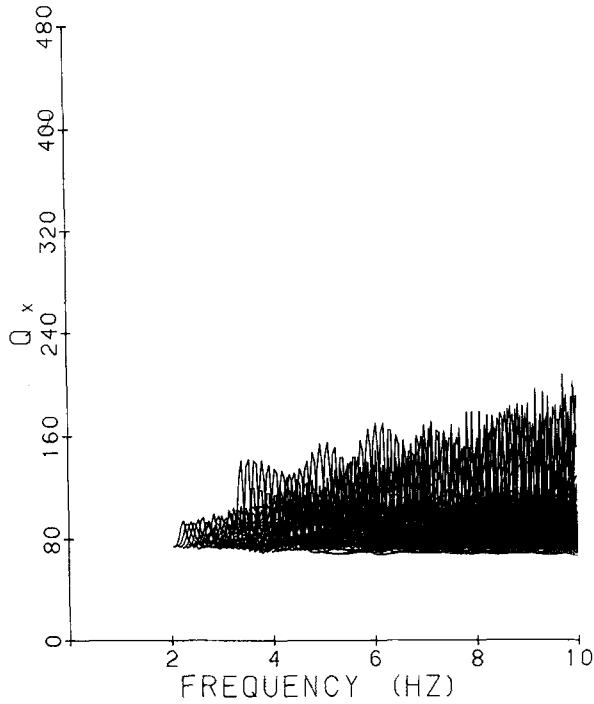


Figure 6b

Figure 6

Love-wave quality factor Q_x for the structure FRIUL7A. The spectrum is divided into two parts: a) Love Modes 0–30, b) Love modes 31–153.

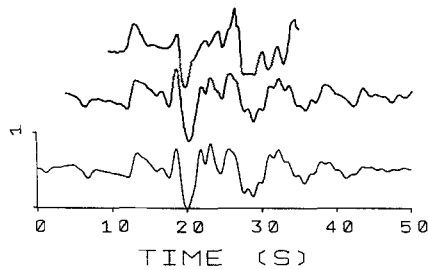


Figure 7

Comparison between the observed ground displacement (top trace), the synthetic signals (middle trace) computed by SWANGER and BOORE (1978) and our synthetics (lowest trace) for the Brawley, 1976 earthquake as recorded at station IVC. For the synthetic signals a vertical right-lateral strike-slip point source with duration of 1.5 s, placed on a vertical plane at 6.9 km depth, is considered. All amplitudes are normalized to a source with a seismic moment of 1 dyne cm. The peak displacement is $6.0 \cdot 10^{-25}$ cm.

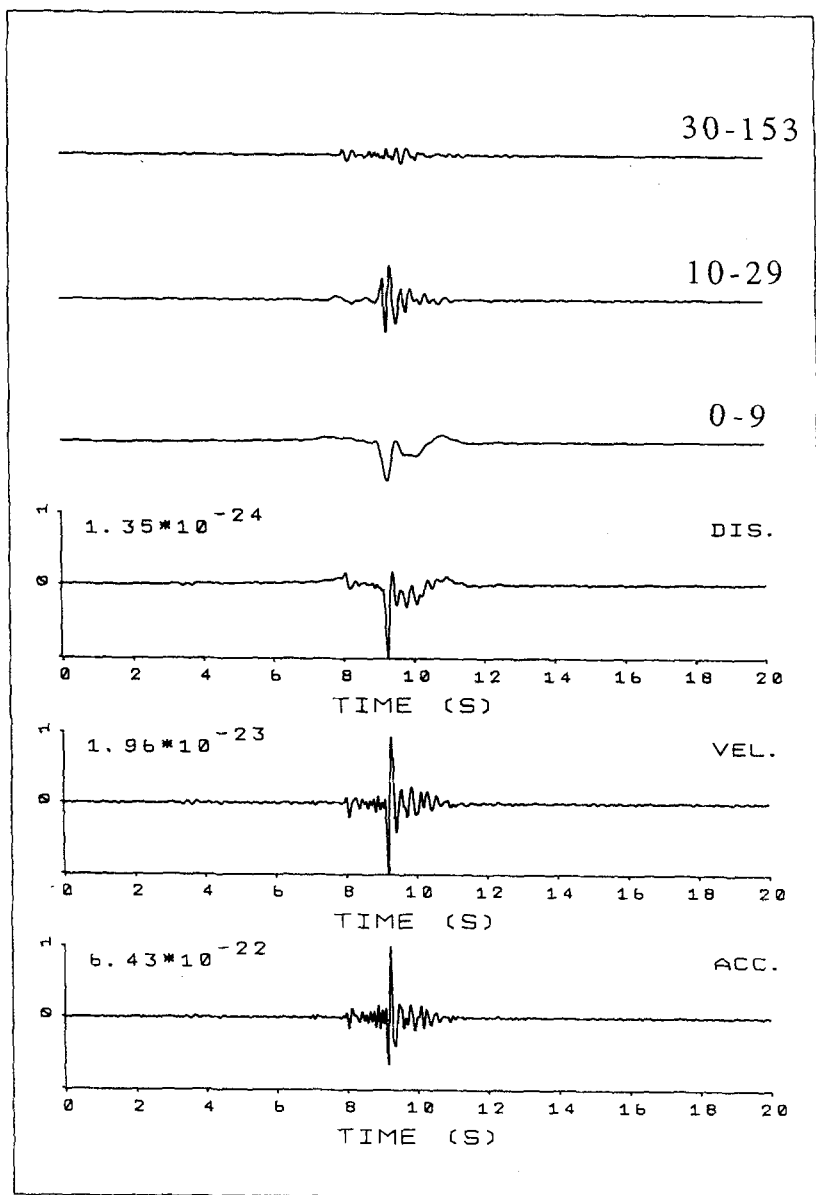


Figure 8

Displacement, velocity and acceleration (lower three traces), computed for a receiver placed 30 km from the source. The displacement is decomposed in different sets of modes (upper three traces: Love modes 30-153, Love modes 10-29, Love modes 0-9). It shows the contribution of the higher modes to the signal waveform. An instantaneous point source with a depth of 7 km is considered (angle strike-receiver $\phi = 280^\circ$, dip $\delta = 30^\circ$ and rake $\lambda = 115^\circ$). All amplitudes are normalized to a source with seismic moment of 1 dyne cm. The peak displacement is in units of cm, the peak velocity in units of cm s^{-1} and the peak acceleration in units of cm s^{-2} .

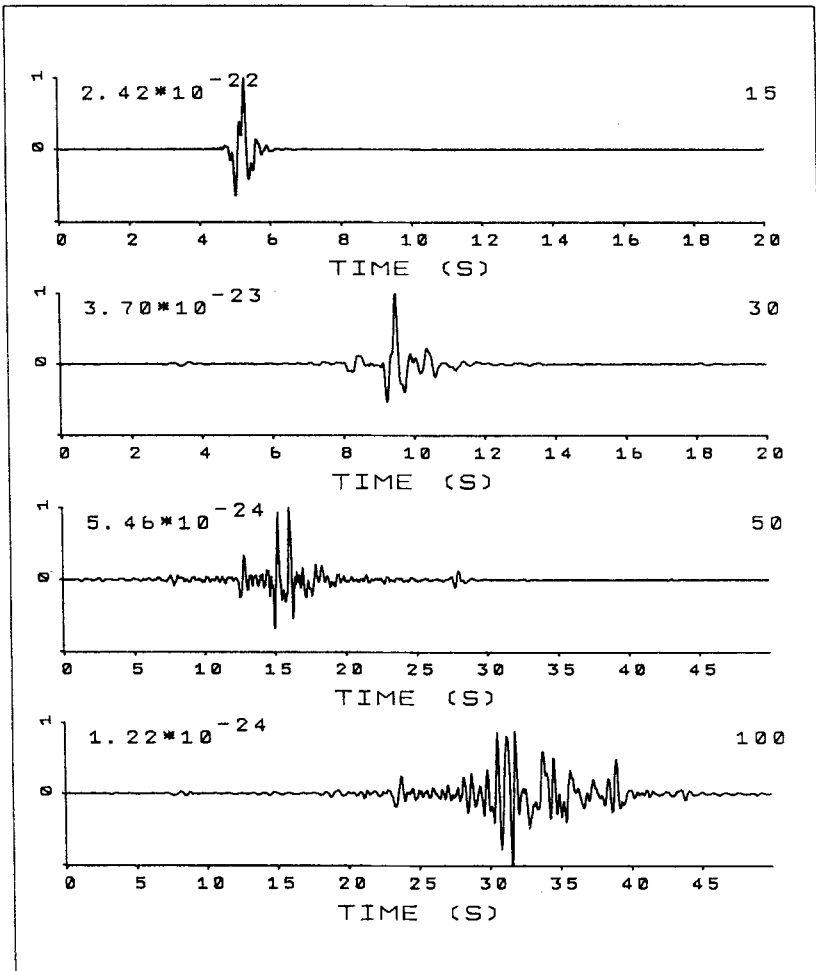


Figure 9

Acceleration time series at different distances from the source (15 km, 30 km, 50 km and 100 km). A point source with duration of 0.5 s and 7 km depth is considered (angle strike-receiver $\phi = 280^\circ$, dip $\delta = 30^\circ$ and rake $\lambda = 115^\circ$). All amplitudes are normalized to a source with seismic moment of 1 dyne cm. The peak acceleration is in units of cm s^{-2} .

strong phases at about 35 s, for the signal at 100 km distance from the source (lowest trace), can be identified as the *Lg* wavetrain.

The last example compares synthetic seismograms and observed data for the September 11, Friuli (Italy) aftershock (16:35). The event has been recorded by various accelerograph stations (CNEN-ENEL, 1977) The three component uncorrected seismograms recorded at the station Buia are shown in Figure 10a.

PANZA and SUHADOLC (1987) have shown, assuming the 1-D layered, anelastic structural model FRIUL7A, that the observed vertical signal at the station Buia

cannot be explained by one point source only. A good fit was obtained with three point sources, having different weights and time shifts, but the same focal depth and mechanism. The same conclusion was drawn by MAO *et al.* (1990) by modeling all three components of the recorded seismograms. In Figure 10b, the results obtained by MAO *et al.* (1990) are shown, where *SH*- and *P-SV*-waves have been combined. The layered *P*- and *S*-wave velocity model (FRIUL7W in Table 3) used in their study is slightly different from the model FRIUL7A. It is based on the result of a damped least-square inversion of arrival time data from local earthquakes (MAO and SUHADOLC, 1990). The differences between FRIUL7A and FRIUL7W are the depth and shape of the upper low-velocity zone, the depth of the sedimentary cover and the quality factors.

To fit the observed seismograms, the source is approximated by a sum of point sources using a trial-and-error technique. The parameters varied in the process are the number of point sources, their origin time and the weights of the single sources. The distance to the receiver, the source depth, the strike, dip and rake are varied, but kept constant for all subevents. All these parameters are adjusted until satisfactory (in the least-square sense) waveform fit was obtained, both in the time and in the frequency domain.

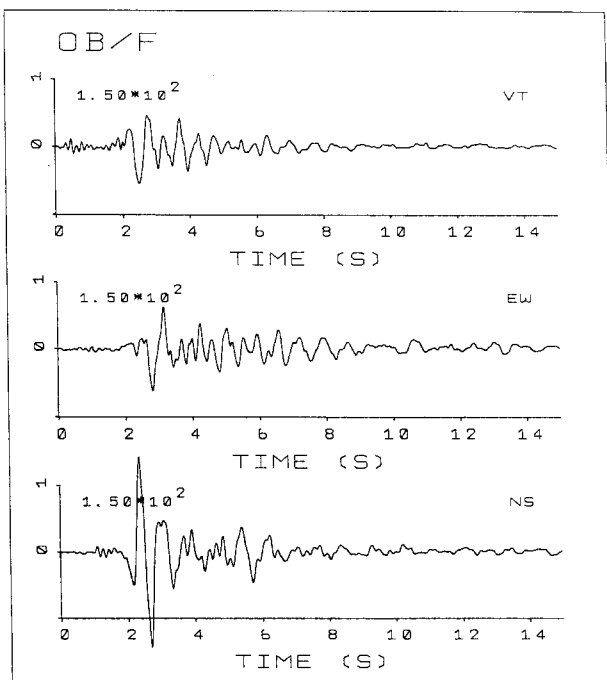


Figure 10a

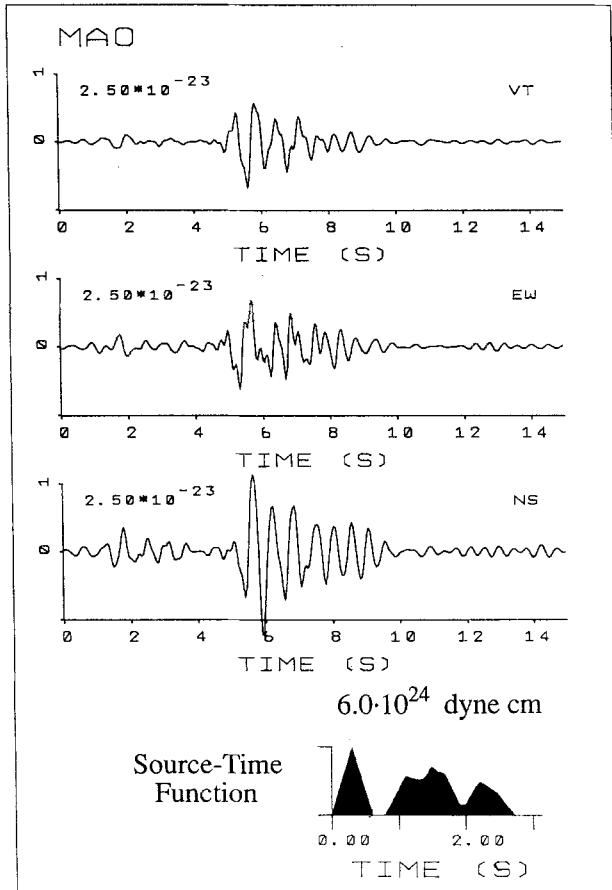


Figure 10b

Figure 10

Comparison of the observed ground motion at the station Buija for the September 11, Friuli aftershock (16:35) with results from waveform fitting with the mode summation technique for a layered, anelastic structure. a) Uncorrected accelerograms, after Gaussian filtering, with a cutoff frequency of 7.5 Hz, for the September 11, Friuli $M_L = 5.7$ aftershock (16:35), observed at the station Buija. The zero of the time axes does not coincide with the origin time. The amplitudes are given in cm s^{-2} . b) Synthetic accelerograms corresponding to six seismic point sources located at the same depth of 17.1 km and the same distance of 15 km (MAO *et al.*, 1990). The strike, the angle between the strike of the source and the receiver, the dip and the rake are 225° , 19° , 28° and 115° , respectively. The six point sources have different weights and time shifts (1.0, 0.6, 0.6, 0.6, 0.5, 0.5 and 0 sec, 0.77 sec, 1.13 sec, 1.37 sec, 1.9 sec, 2.18 sec). In the lowest part of the figure, the normalized source-time function corresponding to the synthetic signals is shown. The seismic moment of $6.0 \cdot 10^{24}$ dyne cm corresponds to the value which gives the best fit of the synthetic to the observed signals.

Table 3
 Structure FRIUL7A. (MAO and SUHADOLC, 1990). Q_α is taken as $2.5Q_\beta$

Thickness [km]	Density [g/cm ³]	P-wave velocity [km/s]	S-wave velocity [km/s]	Q_β
0.057	2.00	1.50	0.60	20
0.043	2.30	3.50	1.80	20
0.20	2.40	4.50	2.50	50
0.70	2.40	5.55	3.05	100
2.00	2.60	5.88	3.24	100
0.10	2.60	5.70	3.14	50
0.20	2.60	5.65	3.10	50
0.20	2.60	5.60	3.06	50
1.00	2.60	5.57	3.03	50
0.50	2.60	5.55	3.02	50
1.00	2.60	5.57	3.03	50
0.20	2.60	5.60	3.06	50
0.20	2.60	5.65	3.10	50
0.10	2.60	5.70	3.14	50
4.50	2.60	5.88	3.25	100
0.10	2.60	6.10	3.40	200
0.10	2.60	6.20	3.50	200
0.10	2.60	6.30	3.60	200
0.70	2.60	6.45	3.75	200
2.50	2.60	6.47	3.77	200
5.00	2.60	6.50	3.80	200
5.00	2.60	6.55	3.82	200
1.00	2.75	6.55	3.82	200
2.00	2.75	7.00	3.85	200
2.00	2.80	7.00	3.85	200
7.50	2.80	6.50	3.75	100
4.00	2.85	7.00	3.85	200
3.00	3.20	7.50	4.25	400
1.50	3.40	8.00	4.50	400
9.00	3.45	8.20	4.65	400

In all cases of waveform fitting, the orientation of the sources agree well with previously published results by SLEJKO and RENNEN (1984), who interpreted the event as a thrust on a very shallow NW dipping plane. To fit the observed signals, several point sources with different weights and time shifts are required. The vertical component and the first phases of the seismograms can be well reproduced, but the NS-component of the synthetic seismograms has too big amplitudes in the coda. The duration of the observed EW component cannot be reproduced with this set of point sources. The station Buia was placed in a sedimentary basin and effects like local surface waves in the basin or two-dimensional resonances can become important. Lateral heterogeneities could therefore account for the differences between the observed and the computed signals for the two horizontal components.

The vertical component of motion is less sensitive to such site-effects, as for example observed at different sites in Mexico City during the 1985 Michoacan earthquake (CAMPILLO *et al.*, 1988). Therefore, considerably better results are obtained for this component.

9. Conclusions

In the case of a layered structure, the mode summation method is a powerful tool to compute synthetic broad-band seismograms. The mode follower and structure minimization allow inclusion of low-velocity zones. Such computations are very efficient and stable. The resulting seismograms include first-order effects due to anelasticity, e.g., the intrinsic attenuation and body-wave dispersion. One of the most attractive aspects of the presented phase and group velocity spectrums is the possibility to identify particular phase arrivals.

One may wonder whether the proposed method is applicable to local structures, which have seldom plane-layer characteristics. In fact, high-frequency seismograms are very sensitive to lateral heterogeneities. Their influence should be included in the numerical modeling. This in turn, requires the use of at least 2-D models to take into account different tectonic settings and site effects. One elegant and efficient way to handle this problem is either by the 2-D mode summation method (VACCARI *et al.*, 1989) for different tectonic settings, or through the combined use of the modal summation method and the finite difference technique (FÄH *et al.*, 1990) for treating site effects.

The mode summation method presented in this paper can be applied in many fields, especially in broad-band studies to analyze recorded regional earthquakes. It can serve to predict radiation patterns of Love waves and can be used in seismic hazard assessments.

Appendix A: Derivatives of the Matrices for the Computation of the Group Velocities

Three cases have to be distinguished: $c > \beta_m$, $c < \beta_m$ and $c = \beta_m$. To avoid excessively heavy notations, layer indexes m and n are dropped. The *S*-wave velocity is denoted by β . Introducing body-wave dispersion, we have:

$$\beta = \frac{B_1(\omega_0)}{1 + \frac{2}{\pi} \cdot B_1(\omega_0) \cdot B_2(\omega_0) \cdot \ln\left(\frac{\omega_0}{\omega}\right)}.$$

$B_1(\omega_0)$ and $B_2(\omega_0)$ are, respectively, the phase velocity and the phase attenuation at the reference angular frequency ω_0 . The rigidity is $\mu = \rho\beta^2$ and ρ is the density. In

the following, d is the layer thickness and k is the wavenumber. Derivatives with respect to c denoted using a dot symbol ($\dot{\cdot}$), while those with respect to ω are denoted with a prime symbol (\prime).

If the halfspace is solid, we use the quantity s (SCHWAB and KNOPOFF, 1972):

$$s = -\mu \cdot \left(1 - \left(\frac{c}{\beta}\right)^2\right)^{1/2}$$

$$\dot{s} = \frac{\partial s}{\partial c} = \frac{\mu \cdot c}{\beta^2 \cdot \left(1 - \left(\frac{c}{\beta}\right)^2\right)^{1/2}}$$

$$s' = \frac{\partial s}{\partial \omega} = \frac{2 \cdot s \cdot B_2(\omega_0) \cdot \beta}{\pi \cdot \omega} \cdot \left(2 + \frac{c^2}{\beta^2 - c^2}\right).$$

If the halfspace is liquid

$$s = \dot{s} = s' = 0$$

while if the halfspace is rigid

$$s = 1 \quad \text{and} \quad \dot{s} = s' = 0.$$

First Case: $c > \beta$

We use here the following notations:

$$r = \left(\left(\frac{c}{\beta}\right)^2 - 1\right)^{1/2}$$

$$Q = \omega \cdot r \cdot \frac{d}{c} = k \cdot r \cdot d.$$

The layer matrix is:

$$b = \begin{bmatrix} \cos Q & \frac{\sin Q}{\mu \cdot r} \\ \mu \cdot r \cdot \sin Q & \cos Q \end{bmatrix}.$$

We have

$$\dot{b}_{11} = -\frac{Q \cdot \beta^2 \cdot \sin Q}{c \cdot (c^2 - \beta^2)}$$

$$\dot{b}_{12} = \frac{1}{\mu} \cdot \left(-\frac{c \cdot \sin Q}{\beta^2 \cdot r^3} + \frac{Q \cdot \beta^2 \cdot \cos Q}{c \cdot r \cdot (c^2 - \beta^2)}\right)$$

$$\dot{b}_{21} = \mu \cdot \left(\frac{c \cdot \sin Q}{\beta^2 \cdot r} + \frac{Q \cdot \beta^2 \cdot r \cdot \cos Q}{c \cdot (c^2 - \beta^2)}\right)$$

$$b'_{11} = -d \left(\frac{r}{c} - \frac{2 \cdot B_2(\omega_0) \cdot c}{\pi \cdot \beta \cdot r}\right) \sin Q$$

$$b'_{12} = \frac{d}{\mu \cdot r} \left(\frac{r}{c} - \frac{2 \cdot B_2(\omega_0) \cdot c}{\pi \cdot \beta \cdot r} \right) \cos Q - \frac{2 \cdot B_2(\omega_0)}{\pi \cdot \beta \cdot r \cdot \rho \cdot \omega} \left(2 - \frac{c^2}{\beta^2 \cdot r^2} \right) \sin Q$$

$$b'_{21} = \mu \cdot r \cdot d \left(\frac{r}{c} - \frac{2 \cdot B_2(\omega_0) \cdot c}{\pi \cdot \beta \cdot r} \right) \cos Q + \frac{2 \cdot B_2(\omega_0) \cdot \mu \cdot \beta \cdot r}{\pi \cdot \omega} \left(2 - \frac{c^2}{\beta^2 \cdot r^2} \right) \sin Q$$

Second Case: $c < \beta$

We use the here the following notations:

$$r = -i \cdot \left(1 - \left(\frac{c}{\beta} \right)^{1/2} \right)^{1/2} \quad \text{with} \quad r = i \cdot r^*$$

$$Q = \omega \cdot r \cdot \frac{d}{c} = k \cdot r \cdot d \quad \text{with} \quad Q = i \cdot Q^*$$

$$Q^* = \omega \cdot r^* \cdot \frac{d}{c}$$

subsequently:

$$\sin Q = i \cdot \sinh Q^*$$

$$\cos Q = \cosh Q^*$$

The layer matrix is:

$$b = \begin{bmatrix} \cosh Q^* & \frac{\sinh Q^*}{\mu \cdot r^*} \\ -\mu \cdot r^* \sinh Q^* & \cosh Q^* \end{bmatrix}$$

We have:

$$\dot{b}_{11} = \frac{Q^* \cdot \beta^2 \cdot \sinh Q^*}{c \cdot (c^2 - \beta^2)}$$

$$\dot{b}_{12} = \frac{1}{\mu} \cdot \left(\frac{c \cdot \sinh Q^*}{\beta^2 \cdot r^{*3}} + \frac{Q^* \cdot \beta^2 \cdot \cosh Q^*}{c \cdot r^* \cdot (c^2 - \beta^2)} \right)$$

$$\dot{b}_{21} = \mu \cdot \left(\frac{c \cdot \sinh Q^*}{\beta^2 \cdot r^*} - \frac{Q^* \cdot \beta^2 \cdot r^* \cdot \cosh Q^*}{c \cdot (c^2 - \beta^2)} \right)$$

$$b'_{11} = d \left(\frac{r^*}{c} + \frac{2 \cdot B_2(\omega_0) \cdot c}{\pi \cdot \beta \cdot r^*} \right) \sinh Q^*$$

$$b'_{12} = \frac{d}{\mu \cdot r^*} \left(\frac{r^*}{c} + \frac{2 \cdot B_2(\omega_0) \cdot c}{\pi \cdot \beta \cdot r^*} \right) \cosh Q^* - \frac{2 \cdot B_2(\omega_0)}{\pi \cdot \beta \cdot r^* \cdot \rho \cdot \omega} \left(2 + \frac{c^2}{\beta^2 \cdot r^{*2}} \right) \sinh Q^*$$

$$b'_{21} = -\mu \cdot r^* \cdot d \left(\frac{r^*}{c} + \frac{2 \cdot B_2(\omega_0) \cdot c}{\pi \cdot \beta \cdot r^*} \right) \cosh Q^*$$

$$- \frac{2 \cdot B_2(\omega_0) \cdot \mu \cdot \beta \cdot r^*}{\pi \cdot \omega} \left(2 + \frac{c^2}{\beta^2 \cdot r^{*2}} \right) \sinh Q^*$$

Third Case: $c = \beta$

Here $r = Q = 0$. Calculations at the limit $c \rightarrow \beta$ are required. The layer matrix becomes:

$$B = \begin{bmatrix} 1 & \frac{\omega \cdot d}{\mu \cdot c} \\ 0 & 1 \end{bmatrix}.$$

We have:

$$\dot{b}_{11} = -\frac{\omega^2 \cdot d^2}{c^3}$$

$$\dot{b}_{12} = -\frac{\omega \cdot d}{\mu \cdot c^2} \cdot \left(1 + \frac{\omega^2 \cdot d^2}{3 \cdot c^2}\right)$$

$$\dot{b}_{21} = \frac{2 \cdot \mu \cdot \omega \cdot d}{c^2}$$

$$b'_{11} = \frac{2 \cdot d^2 \cdot \omega \cdot B_2(\omega_0)}{\pi \cdot c}$$

$$b'_{12} = \frac{d}{\mu} \cdot \left(\frac{1}{c} - \frac{4 \cdot B_2(\omega_0)}{\pi}\right) + \frac{2 \cdot B_2(\omega_0) \cdot \omega^2 \cdot d^3}{3 \cdot \pi \cdot \mu \cdot c^2}$$

$$b'_{21} = -\frac{4 \cdot \mu \cdot d \cdot B_2(\omega_0)}{\pi}.$$

Appendix B: Computation of the Integral Quantities I_1 and C_2 .

The notation *S-L* denotes the transition from the solid to the liquid or rigid halfspace, while the classical solid halfspace will be denoted *S-S*. The dot symbol ($\dot{\cdot}$) is used here for the derivatives with respect to the time. Let us first define the integral J_m^1 , J_m^2 and J_m^3 .

With

$$q_m = k \cdot r_{\beta_m} \cdot (z - z_{m-1})$$

we get:

$$J_m^1 = \int_{z_{m-1}}^{z_m} \cos^2 q_m dz$$

$$J_m^2 = \int_{z_{m-1}}^{z_m} \sin^2 q_m dz$$

$$J_m^3 = \int_{z_{m-1}}^{z_m} \sin q_m \cos q_m dz.$$

We have to distinguish three cases: $c > \beta_m$, $c < \beta_m$ and $c = \beta_m$.

For $c > \beta_m$:

$$J_m^1 = \frac{d_m}{2} + \frac{c \cdot \sin(2Q_m)}{4 \cdot \omega \cdot r_{\beta_m}}$$

$$J_m^2 = \frac{d_m}{2} - \frac{c \cdot \sin(2Q_m)}{4 \cdot \omega \cdot r_{\beta_m}}$$

$$J_m^3 = \frac{c \cdot \sin^2 Q_m}{2 \cdot \omega \cdot r_{\beta_m}}$$

$$J_m^4 = \frac{c \cdot \sin^2 Q_m}{2 \cdot \omega \cdot r_{\beta_m}^2} = \frac{J_m^3}{r_{\beta_m}}$$

$$J_m^5 = r_{\beta_m}^2 \cdot J_m^2; \quad J_m^6 = r_{\beta_m}^2 \cdot J_m^4; \quad J_m^7 = \frac{J_m^2}{r_{\beta_m}^2}.$$

For $c < \beta_m$:

$$J_m^1 = \frac{d_m}{2} + \frac{c \cdot \sinh(2Q_m^*)}{4 \cdot \omega \cdot r_{\beta_m}^*}$$

$$J_m^2 = \frac{d_m}{2} - \frac{c \cdot \sinh(2Q_m^*)}{4 \cdot \omega \cdot r_{\beta_m}^*}$$

$$J_m^3 = \frac{i \cdot c \cdot \sinh^2 Q_m^*}{2 \cdot \omega \cdot r_{\beta_m}^*}$$

$$J_m^4 = \frac{c \cdot \sinh^2 Q_m^*}{2 \cdot \omega \cdot r_{\beta_m}^{*2}} = \frac{J_m^3}{r_{\beta_m}^*}$$

$$J_m^5 = -r_{\beta_m}^{*2} \cdot J_m^2; \quad J_m^6 = -r_{\beta_m}^{*2} \cdot J_m^4; \quad J_m^7 = -\frac{J_m^2}{r_{\beta_m}^{*2}}$$

For $c = \beta_m$:

$$J_m^1 = d_m; \quad J_m^2 = 0; \quad J_m^3 = 0$$

$$J_m^4 = \frac{\omega \cdot d_m^2}{2c}; \quad J_m^5 = 0; \quad J_m^6 = 0; \quad J_m^7 = \frac{\omega^2 \cdot d_m^3}{3c^2}.$$

B1. Energy Integral

The energy integral is:

$$I_1 = \int_0^\infty \rho \cdot \left(\frac{\dot{v}(z)}{\dot{v}_0} \right)^2 dz.$$

For a layered medium, the energy integral can be written:

$$I_1 = \begin{cases} \left(\frac{c}{\dot{v}_0}\right)^2 \cdot \sum_{m=1}^n I_{(m)} & \text{for the (S-L) case} \\ \left(\frac{c}{\dot{v}_0}\right)^2 \cdot \left(\left(\sum_{m=1}^{n-1} I_{(m)}\right) + I_{(S-S)}\right) & \text{for the (S-S) case} \end{cases} \quad (\text{B1})$$

with:

$$I_{(m)} = \int_{z_{m-1}}^{z_m} \rho_m \cdot \left(\frac{\dot{v}(z)}{c}\right)^2 dz \quad (\text{B2})$$

$$I_{(S-S)} = \int_{z_{n-1}}^{\infty} \rho_n \cdot \left(\frac{\dot{v}(z)}{c}\right)^2 dz. \quad (\text{B3})$$

The integrals can be written:

$$I_{(m)} = -\rho_m \cdot k^2 \cdot \left(v_{m-1}^2 \cdot J_m^1 + \frac{(y_{z_{m-1}})^2 \cdot J_m^7}{k^2 \cdot \mu_m^2} + \frac{2v_{m-1} \cdot y_{z_{m-1}} \cdot J_m^4}{k \cdot \mu_m} \right)$$

$$I_{(S-S)} = \frac{\rho_n \cdot v_{n-1}^2 \cdot k}{2 \cdot r_{\beta_n}^*}$$

where v_m is the displacement and y_{z_m} is the stress at the m -th interface.

B2. Phase Attenuation

The coefficient C_2 is given by:

$$C_2 = \frac{\int_0^{\infty} \mu \cdot B_1 \cdot B_2 \cdot \left(\frac{y_z^2}{\mu^2 \cdot k^2} + v^2\right) dz}{c \int_0^{\infty} \mu \cdot v^2 dz}.$$

C_2 can also be written:

$$C_2 = \frac{I^1 + I^2}{c \cdot I^3}$$

with:

$$I^1 = - \int_0^{\infty} \mu \cdot B_1 \cdot B_2 \cdot \left(\frac{\dot{v}}{c}\right)^2 dz = k^2 \cdot v_0^2 \cdot \int_0^{\infty} \mu \cdot B_1 \cdot B_2 \cdot \left(\frac{\dot{v}(z)}{\dot{v}_0}\right)^2 dz$$

$$I^2 = \int_0^{\infty} \mu \cdot B_1 \cdot B_2 \cdot \frac{y_z^2}{\mu^2} dz$$

$$I^3 = - \int_0^{\infty} \mu \cdot \left(\frac{\dot{v}}{c}\right)^2 dz = k^2 \cdot v_0^2 \cdot \int_0^{\infty} \mu \cdot \left(\frac{\dot{v}(z)}{\dot{v}_0}\right)^2 dz.$$

To compute I^1 and I^3 we can use the same scheme as for I_1 in the expression (B1), assuming simple substitution in multiplicative coefficients:

for I^1 we shall use $(\mu_m B_{1_m} B_{2_m} k^2 v_0^2)$ instead of μ_m and
for I^3 we shall use $(\mu_m k^2 v_0^2)$ instead of μ_m .

Let us now consider I^2 . For the *S-L* case, we obtain:

$$I^2 = k^2 \cdot \sum_{m=1}^n \mu_m \cdot B_{1_m} \cdot B_{2_m} L_m$$

while for the *S-S* case, we have:

$$I^2 = \left(k^2 \cdot \sum_{m=1}^{n-1} \mu_m \cdot B_{1_m} \cdot B_{2_m} L_m \right) - \frac{k \cdot \mu_n \cdot B_{1_n} \cdot B_{2_n} \cdot v_{n-1}^2 \cdot r_{\beta_n}^*}{2}.$$

The quantity L_m is given by:

$$L_m = v_{m-1}^2 \cdot J_m^5 + \frac{y_{z_{m-1}}^2 \cdot J_m^1}{k^2 \cdot \mu_m^2} - \frac{2 \cdot v_{m-1} \cdot y_{z_{m-1}} \cdot J_m^6}{k \cdot \mu_m}.$$

REFERENCES

- AKI, K., and RICHARDS, P. G., *Quantitative Seismology* (Freeman and Co., San Francisco, 1980).
- BEN-MENACHEM, A. (1961), *Radiation of Seismic Surface Waves from Finite Moving Sources*, Bull. Seismol. Soc. Am. 51, 401–435.
- BEN-MENACHEM, A., and HARKRIDER, D. G. (1964), *Radiation Patterns of Seismic Surface Waves from Buried Dipolar Point Sources in a Flat Stratified Earth*, J. Geophys. Res. 69, 2605–2620.
- CAMPILLO, M., BARD, P.-Y., NICOLLIN, F., and SANCHEZ-SESMA, F. (1988), *The Mexico Earthquake of September 19, 1985—The Incident Wavefield in Mexico City during the Great Michoacan Earthquake and its Interaction with the Deep Basin*, Earthquake Spectra 4 (3), 591–608.
- CNEN-ENEL (1977), *Uncorrected Accelerograms. Accelerograms from the Friuli, Italy, Earthquake of May 6, 1976 and Aftershocks: Part 3*, Rome, Italy, November 1977.
- DAY, S. M., MCLAUGHLIN, K. L., SKOLLER, B., and STEVENS, J. L. (1989), *Potential Errors in Locked Mode Synthetics for Anelastic Earth Models*, Geophys. Res. Lett. 16, 203–206.
- FÄH, D., SUHADOLC, P., and PANZA, G. F. (1990), *Estimation of Strong Ground Motion in Laterally Heterogeneous Media*, Proc. 9-th European Conf. on Earthquake Eng., Sept. 1990, Moscow, USSR.
- FUTTERMAN, W. I. (1962), *Dispersive Body Waves*, J. Geophys. Res. 67, 5279–5291.
- HARKRIDER, D. G. (1970), *Surface Waves in Multilayered Elastic Media. Part II. Higher Mode Spectra and Spectral Ratios from Point Sources in a Plane Layered Earth Model*, Bull. Seismol. Soc. Am. 60, 1937–1987.
- HARVEY, D. J. (1981), *Seismograms Synthesis Using Normal Mode Superposition: The Locked Mode Approximation*, Geophys. J. R. Astr. Soc. 66, 37–69.
- HASKELL, N. A. (1953), *The Dispersion of Surface Waves in Multilayered Media*, Bull. Seismol. Soc. Am. 43, 17–34.
- HEATON, T. H., and HELMBERGER, D. V. (1978), *Predictability of Strong Ground Motion in the Imperial Valley: Modeling the M4.9, November 4, 1976 Brawley Earthquake*, Bull. Seismol. Soc. Am. 68, 31–48.
- KNOPOFF, L. (1964), *A Matrix Method for Elastic Wave Problems*, Bull. Seismol. Soc. Am. 54, 431–438.
- KNOPOFF, L., SCHWAB, F., and KAUSEL, E. (1973), *Interpretation of Lg*, Geophys. J. R. Astr. Soc. 33, 389–404.
- MAO, W. J., and SUHADOLC, P. (1990), *Ray-tracing, Inversion of Travel Times and Waveform Modelling of Strong Motion Data: Application to the Friuli Seismic Area NE Italy*, Geophys. J. Int. Submitted.

- MAO, W., SUHADOLC, P., FÄH, D., and PANZA, G. F. (1990), *An Example of Interpretation Strong Motion Data by Source Complexity*, 18th International Conference on Mathematical Geophysics, Jerusalem, Israel (17–22 June 1990).
- PANZA, G. F., SCHWAB, F. A., and KNOPOFF, L. (1973), *Multimode Surface Waves for Selected Focal Mechanisms. I. Dip-slip Sources on a Vertical Fault Plane*, *Geophys. J. R. Astr. Soc.* **34**, 265–278.
- PANZA, G. F., and CALCAGNILE, G. (1975), *Lg, Li and Rg from Rayleigh Modes*, *Geophys. J. R. Astr. Soc.* **40**, 475–487.
- PANZA, G. F. (1985), *Synthetic Seismograms: The Rayleigh Waves Modal Summation*, *J. Geophys.* **58**, 125–145.
- PANZA, G. F., and SUHADOLC, P., *Complete strong motion synthetics*. In *Seismic Strong Motion Synthetics* (Bolt, B. A., ed.) (Academic Press, Orlando 1987), *Computational Techniques* **4**, 153–204.
- SCHWAB, F. (1970), *Surface-wave Dispersion Computations: Knopoff's Method*, *Bull. Seismol. Soc. Am.* **60** 1491–1520.
- SCHWAB, F., and KNOPOFF, L. (1971), *Surface Waves on Multilayered Anelastic Media*, *Bull. Seismol. Soc. Am.* **61**, 893–912.
- SCHWAB, F., and KNOPOFF, L., *Fast surface wave and free mode computations*, In *Methods in Computational Physics*, vol. 11 (Bolt, B. A., ed.) (New York, Academic Press 1972) pp. 86–180.
- SCHWAB, F., and KNOPOFF, L. (1973), *Love Waves and Torsional Free Modes of a Multilayered Anelastic Sphere*, *Bull. Seismol. Soc. Am.* **63**, 1103–1117.
- SCHWAB, F., NAKANISHI, K., CUSCITO, M., PANZA, G. F., LIANG, G., and FREZ, J. (1984), *Surface Wave Computations and the Synthesis of Theoretical Seismograms at High Frequencies*, *Bull. Seismol. Soc. Am.* **74**, 1555–1578.
- SCHWAB, F. (1988), *Mechanism of Anelasticity*, *Geophys. J.* **95**, 261–284.
- SLEJKO, D., and RENNER, G. (1984), In “Finalità ed Esperienze della Rete Sismometrica del Friuli-Venezia Giulia”, pp. 75–91. Regione Autonoma Friuli-Venezia Giulia, Trieste.
- SUHADOLC, P., CERNOBORI, L., PAZZI, G., and PANZA, G. F., *Synthetic isoseismal: Applications to Italian earthquakes, Seismic Hazard in Mediterranean Regions*, In J. Bonnin *et al.* (eds.) (Kluwer Academic Press 1988) pp. 205–228.
- SWANGER, H. J., and BOORE, D. M. (1978), *Simulation of Strong-Motion Displacements Using Surface-wave Modal Superposition*, *Bull. Seismol. Soc. Am.* **68**, 907–922.
- TAKEUCHI, H., and SAITO, M., *Seismic surface waves*, In *Methods in Computational Physics*, vol. 11, (Bolt, B. A., ed.) (New York, Academic Press 1972) pp. 217–295.
- THOMSON, W. T. (1950), *Transmission of Elastic Waves through a Stratified Solid Medium*, *J. Appl. Phys.* **21**, 89–93.
- VACCARI, F., GREGERSEN, S., FURLAN, M., and PANZA, G. F. (1989), *Synthetic Seismograms in Laterally Heterogeneous Anelastic Media by Modal Summation of P-SW-waves*, *Geophys. J. Int.* **99**, 285–295.

(Received November 20, 1990, revised/accepted May 30, 1991)